# A field study of the ripple vortex shedding process in the shoaling zone of a macro-tidal sandy beach

**E. Mignot†, D. Hurther††, F-X. Chassagneux††, and J-M. Barnoud††**

† LMFA-INSA Lyon, FRANCE
†† LEGI-CNRS Grenoble, FRANCE
emmanuel.mignot@insa-lyon.fr

**ABSTRACT** ▬▬▬▬▬▬▬▬▬▬▬▬▬▬▬▬▬▬▬▬▬▬▬▬▬▬▬▬

MIGNOT, E., HURTHER, D., CHASSAGNEUX, F-X. and BARNOUD, J-M, 2009. A field study of the ripple vortex shedding process in the shoaling zone of a macro-tidal sandy beach. Journal of Coastal Research, SI 56 (Proceedings of the 10th International Coastal Symposium), pg – pg. Lisbon, Portugal, ISBN

This paper presents an analysis of the field data collected at the French Atlantic coast during the ECORS project on near-shore flow / sediment processes of macro-tidal sandy beaches. An Acoustic Doppler Velocity Profilers has been deployed in the macro tidal region in order to profile the cross-shore and vertical flow velocity components over a distance of 33cm above the bed. For a moderate wave climate, 5cm high ripples were seen to migrate across the acoustic beam in the shoaling zone. We observe that the flow field in the near bed region is strongly affected by the ripples. As previously described in the literature, two flow separation regions exist for each ripple at each wave cycle: a first one on the landward face of the ripple just after the wave crest and a second one on the seaward face during the wave trough. The vertical orbital velocity shows an inversion of sign during each separation and subsequent reattachment phase. Moreover, the orbital stress is calculated as the product of the measured cross-shore and vertical orbital velocities. The characteristic pattern of the orbital stress field differs strongly for both faces of the ripple. Finally, the transverse vorticity field also reveals different behaviors at each face of the ripple. The analysis of the whole set of data reveals the consistency of this orbital stress and vorticity organization, with more intense values encountered near the ripple crest.

**ADITIONAL INDEX WORDS:** *Hydrodynamics, Sandy beach, Orbital stress*

## INTRODUCTION

Ripple-covered beds are common feature across the sandy near-shore regions. They appear in the flow regions where the local Froude number is around its critical value of one. For calm to moderated wave climate conditions this region usually corresponds to the shoaling zone on the seaward face of the wave breaking bar and to the internal surf zone after the energetic wave breaking region. In the swash zone however, ripples are wiped out because of the strong bed friction effects leading to the wash load regime. In the region where ripple formation occurs, a mutual interaction between the ripples and the oscillatory flow takes place. The oscillatory flow makes the ripples migrate landward (VANDERWERF et al., 2007) at a speed being one to two order of magnitudes lower than the applied wave velocities because the ripple shapes are only slightly modified at each wave cycle. In turn, the ripple strongly modifies the near-bed hydrodynamics when flow separation occurs at one or both faces of the ripple crests. In this case, turbulent energy is drastically increased in the near-bed region and the associated ripple vortex entrainment enhances sediment resuspension and cross-shore transport. If the influence of bed ripples on the near-bed hydrodynamics has been studied thoroughly in controlled laboratory conditions, its observation and characterization in the nearshore region still remains poorly documented. This is primarily due to the lack of field deployable flow instrumentation with sufficient spatio-temporal resolution to capture the co-located flow dynamics and bed shape over an extended vertical region above the bed.

Therefore most of the flow data available in the literature concern experimental studies in laboratory conditions with high resolution PIV or laser techniques. Two main types of facilities are used: wave flumes (EARNSHAW and GREATED 1998, FREDSOE et al. 1999, OURMIERES and CHAPLIN 2004, NICHOLS and FOSTER 2007) and oscillatory flow tunnels (VANDERWERF et al. 2007, AHMED and SATO 2001, ADMIRAAL et al., 2006). Moreover, the ripples on the bottom of the flumes are either man-made (with a fixed concrete pre-defined geometry) or self-made (letting the sediment bed organizing itself). All these studies observe the formation of two vortex at the seaward and landward faces of the ripple crest during the passage of the wave crest and wave trough, respectively. These vortex are generated by the flow separation process in the two alternating wake zones where the ripple shape presents strong bed slopes. Prior to both flow reversal phases at each wave cycle, the ripple vortex is then lifted up due to negative velocity gradients giving rise to the so-called "ripple vortex entrainment" process into the water column. (NICHOLS and FOSTER 2007). Then, if the ripple wavelength is comparable to the wave excursion, the coherent vortex can travel towards the neighboring ripples where it can interact with the vortex created locally (EARNSHAW and GREATED 98, ADMIRAAL et al., 06). At each oscillatory cycle, the most energetic vortex seems to be the one over the lee face (landward side) of the ripples as the wave crest passes through with stronger onshore velocities (VANDERWERF et al. 2007).

However, the experimental conditions in which previously described measurements are performed strongly differ from the field conditions. The monochromatic wave field compared to wave field irregularity in nature, the simplified 2D shape of the ripples, the simplified 1D cross-shore propagating wave conditions in the absence of longshore current due to wavefront incidence and/ or rip currents tend to oversimplify the near-bed
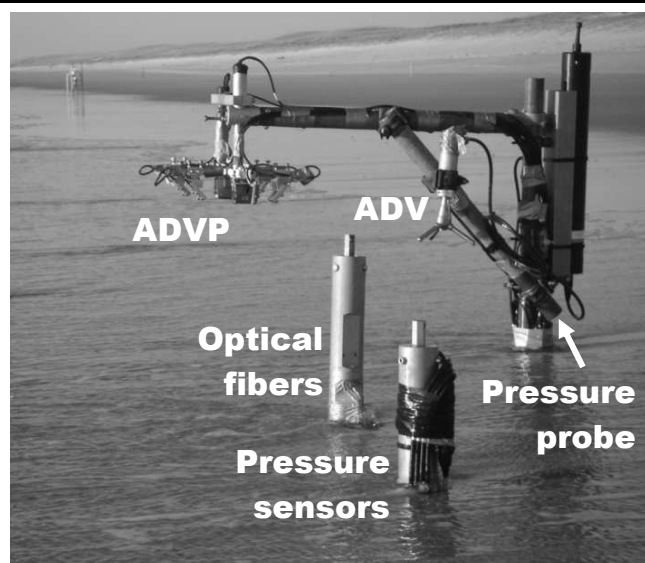
Figure 1. Experimental devices shown at low tide

hydrodynamics. Whether the ripple vortex entrainment still occurs in the much more complex field conditions and what are the impacts on the flow and sediment transport has to be put into evidence before it can be modeled in numerical models. Consequently, during the last decade researchers have started to investigate the on-field near-bed hydrodynamics over rippled beds. SMYTH et al. (2002) used a Coherent Doppler Profiler to measure the cross-shore and vertical velocity fields in the lower 80 cm near the bed, under a water depth of 3-4 m. Using different velocity decomposition methods, the authors computed the orbital and turbulent velocities and showed that the ripple characteristics strongly affect these velocity fields. CHANG and HANES (2004) used an ADV to measure the flow characteristics about 20 cm above a rippled bed with 4m water depth and 1m wave height. The authors observed a vortex generation on the stoss face (seaward side) of the ripple during the wave troughs with offshore velocities, but they did not observe a vortex on its lee face. The authors give two possible reasons for this result: i) the averaged offshore return current in the vicinity of the bed tends to decrease the maximal landward velocities (during wave crests) and ii) the ripple geometric asymmetry which would tend to create larger flow separation on the stoss face.

The velocity fields and vortex shedding processes seem to differ between experimental and on-field measurements due to the additional complexity of the flow in real beaches. The objective of the present study is then to detail the hydrodynamics of on-field
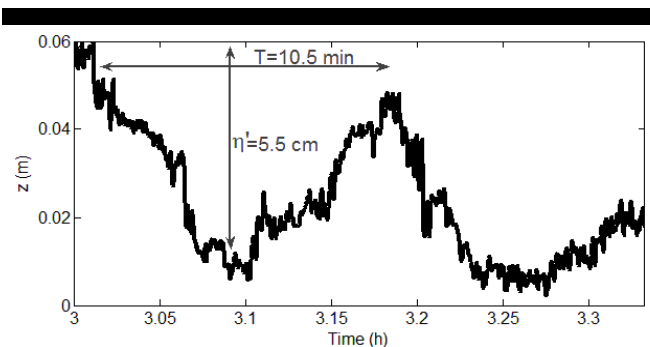


Figure 2. Evolution of bed elevation

measured near-bed flow characteristics.

## EXPERIMENTAL SET-UP AND DATA ANALYSIS

The measurements presented below were collected during the ECORS field campaign (SENECHAL and ARDHUIN, 2008) in March-April 2008 on the Truc-Vert sandy beach at the southern French Atlantic coast. Among other instruments, an Acoustic Doppler Velocity Profiler (ADVP, see HURTHER and LEMMIN (2001, 2008) for a detailed description of its principles, limitations and performances) was deployed in the macro-tidal region of the beach in order to profile the cross-shore and vertical flow velocity components in the near-bed region during high tides. The data analysed in the present paper correspond to a 20 minute sequence (between 3.00 and 3.20 am UT) collected at high tide in the morning of April 5th. In this region of the beach, the flow and beach profile is mainly 2D with negligible influence of the large-scale 3D rip channel located at more than 80m from the measuring point. During this measurement sequence, the water depth was $h=1.7m$ with waves of significant wave height equal to $Hs=0.5m$, and a mean wave period $Ts= 10s$. The ratio $Hs/h$ (being lower than 0.5) shows that the data were collected in the shoaling zone where rippled beds are often observed.

The ADVP (Figure 1) emitted vertical wave trains of frequency $f_0=1MHz$ at a sampling frequency set to 15.6Hz. At each time step, the cross-shore ($u$) and vertical ($w$) instantaneous velocity components were measured simultaneously and at the same locations over a vertical profile of about 33cm over the bed with a typical distance between each measurement volume equal to 3mm. Due to wave velocities exceeding the maximal ADVP velocity range, a simple dealiasing algorithm was necessary for velocity reconstruction. Moreover, the detection of the bed echo allowed to determine the evolution of bed elevation at high frequency with an accuracy of about 3mm. In the end, both the bed elevation and 2D velocity profiles are available at high frequency over bursts of 20 minutes each (only one is discussed herein). Furthermore, a pressure probe has been used to measure the water depth evolution due to waves and tidal excursion (see Figure 1).

At each elevation, both instantaneous zero mean velocity signals $u$ and $w$ were filtered using a low pass filter of 1Hz in order to decompose the measured instantaneous velocities as follows:

$$u - \langle u \rangle = \tilde{u} + u' \qquad (1)$$

with $\langle u \rangle$ the time-averaged, $\tilde{u}$ the orbital and $u'$ the turbulent cross-shore velocity components. The uncertainty in orbital velocity related to the residual turbulent velocity component is of minor importance here since the ripple vortex process is a quasi-cyclic organized flow process at the intra-wave scale. In the following figures, the cross-shore and vertical orbital velocity component $\tilde{u}$ and $\tilde{w}$ are set positive (arrows to the right) for a flow oriented onshore and towards the free surface respectively. The orbital stress is approximated as the product of the orbital vertical and cross-shore velocity components $\tilde{u}\tilde{w}$ since the other terms $\langle \tilde{u}\tilde{w} \rangle$, $\langle u \rangle \tilde{w}$, $\langle w \rangle \tilde{u}$ and $\widetilde{u'w'}$ are neglected.

## RESULTS

### Bed elevation

Figure 2 presents the evolution of bed elevation during the 20 minute time-period. Two oscillation time scales are observed: i) a
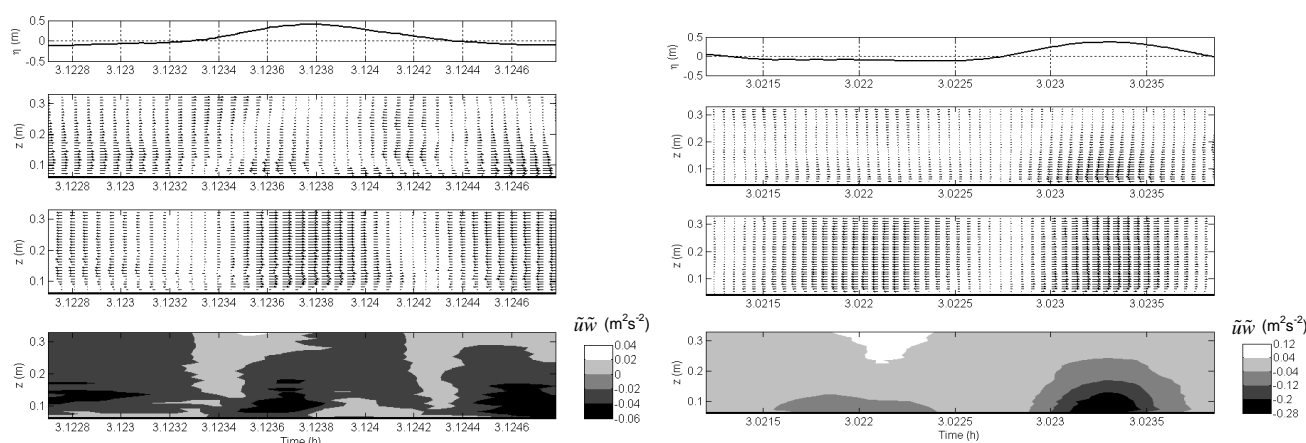
Figure 3. From top to bottom: water depth fluctuation $\eta$ (1), vertical $\tilde{w}$ (2) and cross-shore $\tilde{u}$ (3) orbital velocity fields and orbital stress $\tilde{u}\tilde{w}$ (4) measured over the lee face (left) and stoss face (right) of a ripple.

small time scale of typical period equal to the wave period revealing the impact of each wave on the bed dynamics and ii) a long time scale of typical period *T=10.5min* revealing the presence of two ripples migrating across the acoustic beam of the ADVP. The large time-scale evolution in Figure 2 resembles much with the bed elevation evolution measured by AUSTIN and MASSELINK (2008). The height of the ripples is seen to be equal to *η'=5.5 cm*, which is very close to Nielsen (1981) predictions for a typical wave height *Hs=0.5m* (*η'~6cm*).

It can be seen in Figure 2 that as the ripples migrate landward, the data measured during time periods t=[3;3.1] and [3.18;3.27] (respectively t=[3.1;3.18]) correspond to measurements over the stoss faces (respectively the lee face of the ripples). The flow analysis at these time periods then allows the flow analysis over both faces of the ripples.

## Orbital velocity field and orbital stress

Previous experimental and field studies showed that the velocity field above a rippled bed is strongly influenced by the local topography over a depth up to 5 times the ripple height. Figure 3 presents the water surface elevation, the cross-shore, the vertical velocity fields and the orbital stress field over a given wave cycle when the ADVP is above the lee face (left hanside) and stoss face (right handside) of a ripple. It appears that the cross-shore orbital

velocity profiles are well correlated with the water depth fluctuation $\eta$ with stronger vertical gradient in the near-bed region. For positive $\eta$ values (water depth larger than its mean value), the flow is oriented landward and for negative $\eta$ values, the flow is oriented seaward. Concerning the vertical velocity profiles, two distinct behaviors are observed. In the upper part of the profiles (*z>0.3m*), $\tilde{w}$ is positive when the water depth increases (from wave trough to wave crest) and is negative when the water depth decreases following the linear wave theory. On the other hand, in the lowest 30cm of the flow (equivalent to 5-6 ripple heights), the sign of the vertical velocity is strongly affected by the presence of the ripple:

* Over the lee face of the ripple (Figure 3, left), the vertical velocity is negative prior to the wave crest with a maximum negative velocity measured very close to the bed and it is positive prior to and during the wave trough with maximum positive velocity measured at the bed. This near-bed behavior is strongly linked with vortex shedding over the ripple: i) Just after the wave crest, the landward flow separates from the bed over the ripple lee face with positive vertical velocities at the bed. ii) During the wave trough, the seaward flow climbs up along the lee face with still positive vertical velocities. iii) Finally, after the trough-crest flow reversal and at the wave crest, the landward flow descends along the ripples lee face with negative vertical velocities until it
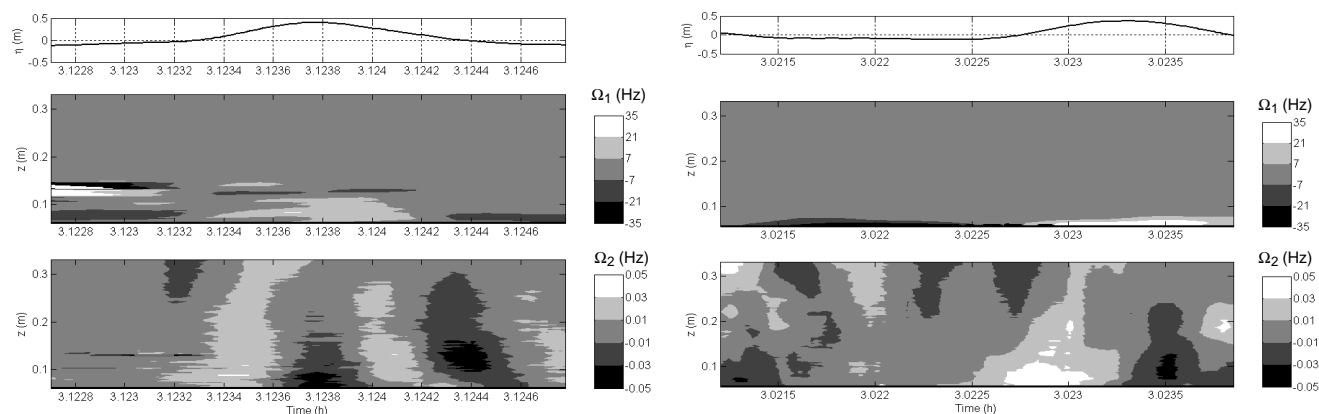


Figure 4. From top to bottom: water depth fluctuation $\eta$ (1), $\Omega_1$ (2) and $\Omega_2$ (3) vorticity terms measured over the lee face (left) and stoss face (right) of a ripple.
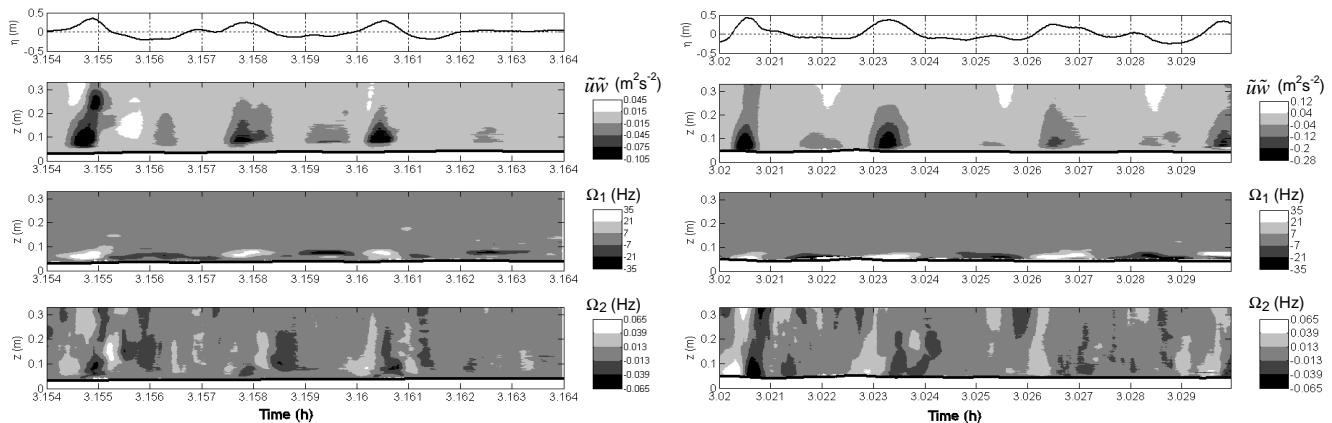
Figure 5. From top to bottom: water depth fluctuation $\eta$ (1), orbital stress $\tilde{u}\tilde{w}$ (2), $\Omega_1$ (3) and $\Omega_2$ (4) vorticity terms measured over the lee face (left) and stoss face (right) near the crest of a ripple (see Figure 2 for location with regards to ripples).

separates again after the following wave crest.

* Over the stoss face of the ripple (Figure 3, right), the vertical velocity is positive during the wave trough and is negative during the wave crest (with maximum adverse velocities observed very close to the bed). Again this near-bed behavior is strongly linked with vortex shedding over the ripple: i) Prior to and during the wave trough, the seaward flow separates from the bed over the ripple stoss face with positive vertical velocities. Then prior to and during the wave crest the flow reattaches the bed with negative vertical velocities.

The inversion of sign of the vertical orbital velocity components along the vertical profiles was already observed by SMYTH et al. (2002, Figure 2b) over rippled beds, although it was not discussed by the author and was not related to vortex shedding.

The direction of cross-shore velocity and upper vertical velocity fields are in fair agreement with the linear wave theory while the direction of the near-bed vertical velocities is determined by the ripple vortex shedding. As a consequence, the orbital stress sign also becomes strongly influenced by the ripple impact on near-bed hydrodynamics:

* Figure 3 (left) shows that over the lee side of the ripple, two upper positive and two near-bed negative orbital stress regions are observed during the wave period: i) at the top of the measured profile (z~0.3m), $\tilde{u}\tilde{w}>0$ prior to the wave crest (as $\tilde{u}>0$ and

$\tilde{w}>0$) and prior to the wave trough (as $\tilde{u}<0$ and $\tilde{w}<0$), while ii) in the near-bed region, $\tilde{u}\tilde{w}<0$ prior to the wave crest (as $\tilde{u}>0$ and $\tilde{w}<0$) and prior to the wave trough (as $\tilde{u}<0$ and $\tilde{w}>0$).

* Over the ripple stoss face, one upper large positive orbital region and two near-bed negative orbital stress regions are observed during a wave period: i) at the top of the measured profile, $\tilde{u}\tilde{w}>0$ prior to and during the wave trough (as $\tilde{u}<0$ and $\tilde{w}<0$), while ii) in the near-bed region, $\tilde{u}\tilde{w}<0$ during the wave trough (as $\tilde{u}<0$ and $\tilde{w}>0$) and during the wave crest (as $\tilde{u}>0$ and $\tilde{w}<0$).

In the end, two flow separations are observed, one over each ripple face occurring at the oscillatory half cycle as described in most experimental works. However, it is interesting to note that the separation above the stoss-face is more intense and reaches higher elevations than the one over the lee face (see Figure 3). This result differs from most experimental study conclusions but is consistent with Chang and Hanes (2004) observations described above.

## Transverse (longshore) vorticity field

As for the orbital stress, the vorticity field is strongly affected by the vortex shedding proccesses over rippled beds. The local tranverse (longshore) vorticity component $\Omega$ can be written as:
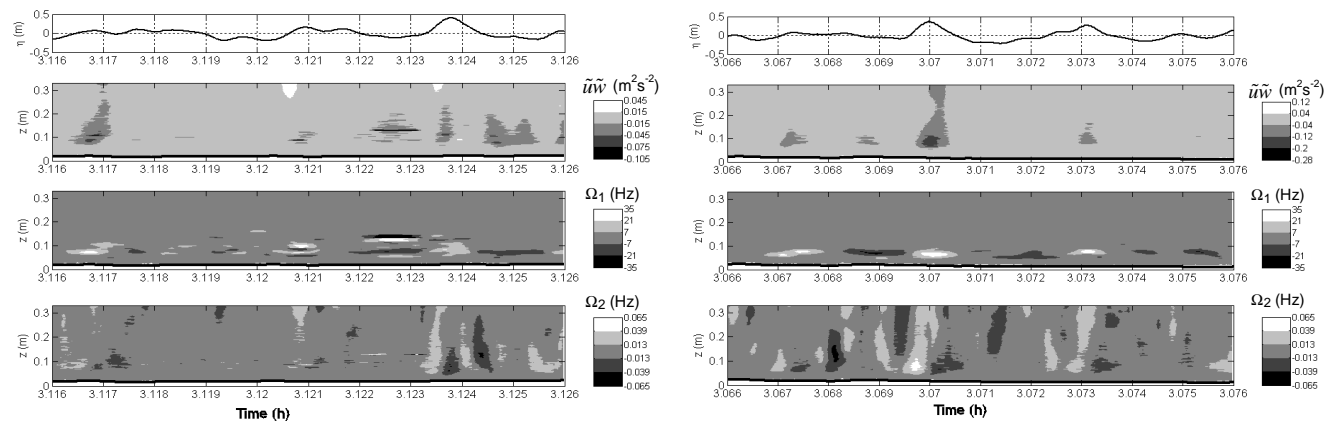


Figure 6. idem Figure 5 near the trough of the ripple (see Figure 2 for location with regards to ripples).

$$\Omega = \Omega_1 + \Omega_2 \qquad (2)$$

with $\Omega_1 = \partial \tilde{u}/\partial z$ and $\Omega_2 = -\dfrac{\partial \tilde{w}}{\partial x} = -\dfrac{1}{\sqrt{gh}}\dfrac{\partial \tilde{w}}{\partial t}$

where $x$ and $z$ are the cross-shore and vertical directions respectively and $h=1.7m$.

Figure 4 shows the vorticity field measured over the lee and stoss faces of a ripple during the same wave periods as in Figure 3. It appears that in both cases, $\Omega_1 >> \Omega_2$. $\Omega_1$ is linked to the cross-shore velocity field and its behaviour is then similar for both faces of the ripples: $\Omega_1 > 0$ below the wave crests as the cross-shore velocity goes from zero at the bed to a strong positive value outside the boundary layer and $\Omega_1 < 0$ below the wave troughs as the cross-shore velocity goes from zero at the bed to a strong negative value above. The strong positive and negative $\Omega_1$ values at $t=3.1228h$ in Figure 4 are only related to measurements uncertainties near $z=0.12m$ in Figure 3. Opositely, given that $\tilde{w}$ field differs (see Figure 3) between the lee and stoss faces of the ripple, $\Omega_2$ field also differs. Over the ripple lee face, $\Omega_2$ (near the bed) is alternatively positive prior to the wave crest, negative at the wave crest, positive prior to crest-trough flow reversal and again negative during this flow reversal. Over the ripple stoss face, $\Omega_2$ (near the bed) is alternatively positive after the trough-crest flow reversal and negative prior to and after crest-trough flow reversal. These signs are of course in direct link with the evolution of $\tilde{w}$ sign in the near-bed region described above.

## Orbital stress and vorticity over longer periods

The objective of this last section is to check whether the specific hydrodynamic observations observed above both faces of the ripples in Figures 3 and 4 are consistent over any type of wave and any position along the ripple faces. Figures 5 and 6 show the orbital stress and vorticity fields over longer periods (typically 3 wave periods) when the measurement device is located near the ripple crest (Figure 5) and near the ripple trough (Figure 6).

Figure 5 shows that the orbital stress and vorticity specific behaviour are consistent over the 3 wave periods even with a strongly irregular wave climate. The positive and negative orbital stress and vorticity regions appear in the same locations with regards to the wave periods. For instance, over the ripple stoss face, both negative orbital stress regions encountered near the bed (during wave crest and wave trough) and the long positive stress observed in the upper measured profile (during the wave trough) are observed at each wave period.

Figure 6 reveals that this very active vortex shedding hydrodynamics near the crest of the ripples, is also encountered in the near-ripple trough region. Nevertheless, the magnitude of the orbital stress and vorticity terms are strongly reduced, which confirms that the main vortex shedding region occurs at the crest of the ripples and dissipates when traveling toward the ripple troughs.

## CONCLUSION

The aim of the present paper was to analyse the existence in field conditions of the ripple vortex shedding process over a migrating rippled bed in the shoaling zone of a macro-tidal beach. An Acoustic Doppler Velocity Profilers was deployed in the macro tidal region of a sandy beach at the French Atlantic coast in order to profile the near-bed cross-shore and vertical flow velocity fields. Two flow separations events have been observed as seen in laboratory experiments: one on the landward (lee) face of the ripple just after the wave crest and the second one on the seaward

(stoss) face during the wave trough. Consequently, the characteristic patterns of the orbital stress and vorticity fields differ strongly for both faces of the ripple. The analysis of the whole set of data reveals the consistency of these flow patterns for irregular waves, with more intense values encountered near the crest of the ripples than near their troughs.

## LITERATURE CITED

ADMIRAAL, D., MUSALEM-JARA, R., GARCIA, M., and NINO, Y., 2006. Vortex trajectory hysteresis above self-formed vortex ripples. *Journal of Hydraulic Research*, 44(4), 437-450.

AHMED, A.S.M. and SATO, S., 2001. Investigation of bottom boundary layer dynamics of movable bed by using enhanced PIV technique. *Coastal Engineering*, 43, 239-258.

AUSTIN, J.M. and MASSELINK, G., 2008. The effect of bedform dynamics on computing suspended sediment fluxes using optical backscatter sensors and current meters. *Coastal Engineering*, 55, 251-260.

CHANG, Y.S. and HANES, D.M., 2004. Suspended sediment and hydrodynamics above mildly sloped along wave ripples. *Journal of Geophysical Research*, 109, C07022.

EARNSHAW, H.C. and GREATED, C.A., 1998. Dynamics of ripple bed vortices. *Experiments in Fluids*, 25, 265-275.

FREDSØE, J., ANDERSEN, K.H., and SUMER, B.M., 1999. Wave plus current over a ripple-covered bed. *Coastal Engineering*, 38, 177-221.

HURTHER, D., AND LEMMIN, U., 2001. A correction method for turbulence measurements with a 3D acoustic Doppler velocimetry profiler. *Journal of Atmospheric and Oceanic Technology*, 18(3), 446-458.

HURTHER, D., AND LEMMIN, U., 2008. Improved turbulence profiling with field adapted acoustic Doppler velocimeters using a bi-frequency Doppler noise suppression method. *Journal of Atmospheric and Oceanic Technology*, 25(2), 452-463.

NICHOLS, C. S., and FOSTER, D.L., 2007. Full-scale observations of wave-induced vortex generation over a rippled bed. *Journal of Geophysical Research*, 112, C10015.

NIELSEN, P., 1981. Dynamics and geometry of wave generated ripples. *Journal of Geophysical Research*, 86, 6467-6472.

OURMIÈRES, Y. and CHAPLIN, J.R., 2004. Visualizations of the disturbed-laminar wave-induced flow above a rippled bed. *Experiments in Fluids*, 36, 908-918.

SENECHAL, N. and ARDHUIN, F, Ecors-truc vert 2008: Qualification des modèles de houle et de morphodynamique. *X° journées nationales Génie civil – Génie côtier* (Sophia-Antipolis, France), in French.

SMYTH, C., HAY, A.E., and ZEDEL, L., 2002. Coherent Doppler Profiler measurements of near-bed suspended sediment fluxes and the influence of bed forms. *Journal of Geophysical Research*, 107, C8.

VANDERWERF, J.J., DOUCETTE, J.S., O'DONOGHUE, T., and Ribberink, J.S., 2007. Detailed measurements of velocities and suspended sand concentrations over full-scale ripples in regular oscillatory flow. *Journal of Geophysical Research*, 112, F02012.